Effects of target heating on experiments using $K\alpha$ and $K\beta$ diagnostics

P. Palmeri,[1,*] G. Boutoux,[2,†] D. Batani,[2,‡] and P. Quinet[1,3,§]

[1]*Astrophysique et Spectroscopie, Université de Mons–UMONS, B-7000 Mons, Belgium*

[2]*Univ. de Bordeaux, CNRS, CEA, CELIA (Centre Lasers Intenses et Applications), UMR 5107, F-33405 Talence, France*

[3]*IPNAS, Université de Liège, B-4000 Liège, Belgium*

(Received 14 April 2015; revised manuscript received 7 July 2015; published 29 September 2015)

We describe the impact of heating and ionization on emission from the target of $K\alpha$ and $K\beta$ radiation induced by the propagation of hot electrons generated by laser-matter interaction. We consider copper as a test case and, starting from basic principles, we calculate the changes in emission wavelength, ionization cross section, and fluorescence yield as Cu is progressively ionized. We have finally considered the more realistic case when hot electrons have a distribution of energies with average energies of 50 and 500 keV (representative respectively of "shock ignition" and of "fast ignition" experiments) and in which the ions are distributed according to ionization equilibrium. In addition, by confronting our theoretical calculations with existing data, we demonstrate that this study offers a generic theoretical background for temperature diagnostics in laser-plasma interactions.

DOI: 10.1103/PhysRevE.92.033108 PACS number(s): 52.38.Ph, 52.70.La, 52.50.Jm, 32.30.Rj

I. INTRODUCTION

$K\alpha$ emission from tracer layers, or dopants, embedded in laser-irradiated targets has long been used as a diagnostic of the presence and the propagation of hot electrons produced in laser-matter interaction. In the typical experimental setup used in most experiments (see Fig. 1), the high-intensity short-pulse laser [obtained through chirped pulse amplification (CPA)] is focused on the surface of the target where the fast electrons are produced and accelerated inside the material. They cross a first "propagation layer" and then arrive at one or two $K\alpha$ fluor layers where they induce the emission of $K\alpha$ photons. By varying the thickness of the propagation layer it is possible to reconstruct the typical penetration range of the fast electrons. After the fluor layers, an additional plastic layer may be placed. This will prevent any spurious $K\alpha$ emission due to fast electrons which go around the target or which have crossed the targets and are pulled back towards it by electrostatic forces.

The use of two (or more) fluor layers should be preferred to the use of a single layer. Indeed the number of $K\alpha$ emitted photons will mainly depend on two parameters: the initial number of fast electrons and their energy (which fixes the propagation range). Hence, in principle, the use of two tracer layers will allow these two parameters to be determined shot by shot. Also, in the limit in which only collisional effects are important (stopping power limit), the ratio of $K\alpha$ yield from the two layers will be independent of the initial number of fast electrons and dependent only on their energy.

$K\alpha$ emission was first observed in the pioneering early work of Zigler *et al.* [1] and Key *et al.* [2]. $K\alpha$ tracer layers were also used in connection with the first observation of collective effects (due to resistive electric fields) in hot electron penetration in matter in 1982, i.e., long before the advent of short-pulse high-intensity lasers. In this experiment Bond *et al.* [3] used a gold foam target. Since collisional effects are proportional to target density, the stopping power is sensitive only to the total areal mass density of the target, $m = rd$. Hence using low-density foams is a good method of affecting the relative weight of electric field effects with respect to collisional ones.

Depending on the laser intensity on the target and on the laser duration, hot electrons are produced by several mechanisms like resonant absorption [4], parametric instabilities [5] [stimulated Raman scattering (SRS) and two-plasmon decay (TPD)], and, at higher laser intensity by direct ponderomotive acceleration (including the so-called $J \times B$ effect) [6] or by the Brunel effect (quasiresonant absorption) [7].

Once generated, the hot electrons penetrate into the target material and produce inner shell ionization by collisions. Such inner holes are then filled in by radiative recombination, emitting the characteristics line of the elements of the material. This process is in competition with emission of Auger electrons, and the branching ratio between these two processes is called the fluorescence yield of the material (which is a function of its atomic number Z).

As said above, the emission of characteristic lines (usually the $K\alpha$ line) can be used for various diagnostics. First, by putting tracer layers at different depths inside the target, one can infer the propagation range of hot electrons in matter, which provides measurements of the hot electron temperature (at least as long as collective effects do not influence the propagation). More recently, imaging techniques, in particular based on spherically bent x-ray crystals [8–10] have also been used, which provide information on the spatial shape of the $K\alpha$ source, which is related to the spatial shape of the beam of hot electrons as they cross the tracer layer.

A more sophisticated variant of $K\alpha$ diagnostics is $K\alpha$ spectroscopy [11–13]. This is based on the fact that, when material is heated by the passage of fast electrons, atoms are ionized and subsequent $K\alpha$ radiation has a shifted wavelength depending on the ionization state of the emitting ions. More recently $K\beta$ radiation has also been used [14] since $K\beta$ spectroscopy provides easier separation of the satellite lines and at lower ionization states in comparison with $K\alpha$ spectroscopy. This feature allows measuring the temperatures of relatively cold matter, even for high-Z materials. Usually, in

*Corresponding author: patrick.palmeri@umons.ac.be
†boutoux@celia.u-bordeaux1.fr
‡batani@celia.u-bordeaux1.fr
§pascal.quinet@umons.ac.be

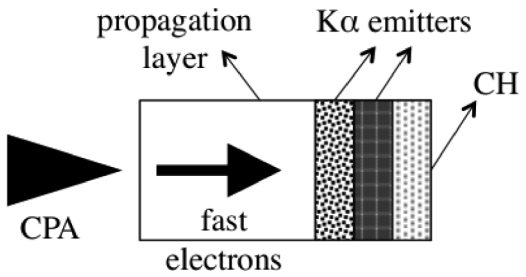

FIG. 1. Typical experimental setup for measuring the penetration range of fast electrons through $K\alpha$ spectroscopy.

K-shell spectral analysis, the plasma temperature and density are inferred from fitting predictions from available atomic models to the measured data.

The goals of this paper are to evaluate the effects of the induced ionization on shift of the $K\alpha$ and $K\beta$ lines, but also to evaluate the effects of the changes induced in the ionization cross section and fluorescence yield when tracer atoms become ionized. While the first effect has already been seen in the past and described in the literature, this study also takes into account the changes in cross section and fluorescence yield. Our goal is not to try to reproduce the data from one or another experiment exactly; rather we want to show the influence of the studied processes using simple "academic" cases.

II. IMPORTANCE OF Cu TRACER AS A TEST CASE

In the following we will refer to Cu as a "test" case, since this has been used as a tracer element in many experiments. Indeed it is very difficult to cite all the articles which are using Cu tracer layers or Cu dopants to trace the propagation of hot electrons in matter.

Some early works date back to the 1980s and were concentrated on use of $K\alpha$ emission to trace the hot electrons and see the effects of lateral energy transport out of the focal spot in either planar [15] or spherical targets [16]. In some cases these experiments were performed at long irradiation wavelength (first harmonics of a Nd:laser or even a CO_2 laser) since long wavelengths are well known to maximize hot electron generation even at laser intensities which are relatively low.

With the advent of short-pulse very-high-intensity lasers based on the CPA technique, relativistic electrons could be created at energies up to a few MeV. A lot of studies on fast-electron propagation in matter have been conducted, mainly in the framework of the fast-ignition approach to inertial fusion.

Several works were addressed at assessing the impact of collective effects on transport of fast electrons, i.e., the effects induced by the self-generated electric and magnetic fields, and the relation with the electrical conductivity of the target material. Typically propagation in metal vs insulator targets allowed such effects to be discriminated [17,18]. Other works concentrated on studying the effects of the influence of the "preplasma" created before the solid target by the laser prepulse [19,20], or the divergence of the fast-electron beam [21]. The role of electron refluxing was studied in [22]. Finally Cu $K\alpha$ emission was also used as a diagnostic of fast electrons in experiments using cone-guiding targets (one of the most studied variants of fast ignition) either in spherical integrated experiments with imploding targets [23], in planar experiments using cone targets [24], or in the configuration of a wire attached to a cone [25].

In addition, the use of Cu $K\alpha$ photons as diagnostics of fast electrons received a big impulse due to the introduction of imaging techniques. This was largely due to the fact that for Cu $K\alpha$ radiation ($\approx$8 keV) spherically bent crystals are available, allowing a very good spatial resolution to be achieved (better than 10 μm in the best conditions). The development of such imaging techniques is largely due to the work of Faenov, Pikuz and co-workers [8–10]. It allowed getting high-resolution images of Cu $K\alpha$ sources and has provided much more insight into the physics of electron transport. For instance, the technique has been applied to study electron beam collimation or spreading in matter compressed by cylindrical implosions [26] and to compare transport of fast electrons in insulators vs metals and assess the effects of collective effects and beam filamentation [27]. Indeed it was the very small spectral acceptance of spherical crystals which drove attention to the $K\alpha$ shift as matter is heated and ionized. The $K\alpha$ shift implied a strong reduction of the collected $K\alpha$ signal even in conditions when this was expected to increase. This was typical, for instance, of experiments done even recently on the Omega laser. Higher pulse energy should correspond to larger $K\alpha$ yield but indeed the collected signal was smaller: more electrons imply a stronger heating of tracer atoms and therefore their emission was shifted outside the crystal spectral range [28]. As a result, this has also driven attention to the use of $K\alpha$ spectroscopy, i.e., assessment of the temperature reached in the background target by looking at the $K\alpha$ line shape and $K\alpha$ wavelength shift as a results of thermally-induced heating [11–13]. Of course, this has attracted interest also to the use of $K\beta$ emission as a complementary diagnostic [14]. Finally, Cu tracer layers have recently been used in experiments related to shock ignition, at subrelativistic laser intensities and with hot-electron energies in the range 30–100 keV [29,30].

As we have already said, such a large number of papers using a Cu tracer (and indeed many more) justifies our attention to copper $K\alpha$ emission. Nevertheless let us again stress the fact that here we do not want to reproduce data from any particular experiment, but rather describe the physical trends.

III. K-SHELL EMISSION MODELING AND ATOMIC DATA USED

In the present study, we considered that the Cu K-shell emission is due entirely to a two-step atomic process, where a K-vacancy level of an ion of charge state Z^*, i.e. the atomic number, $Z = 29$ minus the number of bound electrons, is populated from the ground level of the parent ion of charge state $Z^* - 1$ by fast-electron impact ionization in the first step, and then decays through either a radiative ($K\alpha$ or $K\beta$ transition) or an Auger transition (KLL, KLM, or KMM channel) in a second step. In this model, the number of x-ray photons per unit of time per unit of volume in a particular K line ($K\alpha$ or $K\beta$) of an ion of charge state Z^*, $N(K\alpha \text{ or } K\beta, Z^*)$, will be proportional to the product of the total K-shell electron impact ionization cross section of the ground level of the parent ion, $\sigma_K(E;\ Z^* - 1)$, and the K-shell fluorescence yield for that

particular line, $Y(K\alpha \text{ or } K\beta, Z^*)$, i.e.:

$$N(K\alpha \text{ or } K\beta,\ Z^*) \propto\ \sigma_K(E;\ Z^* - 1) Y(K\alpha \text{ or } K\beta,\ Z^*), \quad (1)$$

where E is the kinetic energy of the fast electron, and the coefficient of proportionality is equal to the product of the velocity and the number per unit of volume of fast electrons with kinetic energy E by the number of ions of charge state $Z^* - 1$ per unit of volume.

The fluorescence yield for a particular K line, $Y(K\alpha \text{ or } K\beta, Z^*)$, is in turn defined as a branching ratio of atomic transition probabilities of the decay branch $X, A(X)$, as follows:

$$Y(K\alpha \text{ or } K\beta,\ Z^*) = \frac{A(K\alpha \text{ or } K\beta,\ Z^*)}{A(K\alpha,\ Z^*) + A(K\beta,\ Z^*) + A(KLL,\ Z^*) + A(KLM,\ Z^*) + A(KMM,\ Z^*)} \quad (2)$$

The copper atomic data involved in Eqs. (1) and (2) were taken from Palmeri *et al.* [31,32] and averaged, as they are given for all charge states up to Li-like Cu in Refs. [31,32] for fine-structure atomic energy levels and not for atomic shells.

The average K-shell fluorescence yields $Y(K\alpha \text{ or } K\beta, Z^*)$ have been estimated using the following formula:

$$Y(K\alpha \text{ or } K\beta,\ Z^*) = \frac{\sum_{i,\,j} Y(i,\ j,\ Z^*)}{n(Z^*)}\ , \quad (3)$$

where the summation runs over all $K\alpha$ or $K\beta$ fine-structure $i \rightarrow j$ transitions emitted from all the upper K-vacancy levels i populated by K-shell electron impact ionization (KEII) from the parent ion ground level, these K-vacancy levels are given as daughter ion fine-structure level indices in Table 2 of Ref. [31], and $n(Z^*)$ is the total number of upper K-vacancy levels populated by the KEII atomic process. The fine-structure fluorescence yields $Y(i, j, Z^*)$ that appear in Eq. (3) have been calculated using the radiative transition probabilities $A_r(i,\ j,\ Z^*)$, and the Auger widths, $A_a(i,\ Z^*)$, published by Palmeri *et al.* [31] following the equation given below:

$$Y(i,\ j,\ Z^*) = \frac{A_r(i,\ j,\ Z^*)}{\sum_{k<i} A_r(i, k,\ Z^*) + A_a(i,\ Z^*)}\ , \quad (4)$$

where the summation in the denominator runs over all the radiative decay channels from the upper K-vacancy fine-structure level i.

In Fig. 2, the average fluorescence yields are given as functions of the charge state Z^* for the $K\alpha$ and $K\beta$ transition arrays. A slight decrease of the $K\alpha$ fluorescence yield for Z^* up to 12 is observed with a corresponding increase of the $K\beta$ fluorescence yield. For $Z^* > 12$, the trends are inverted, with an increase of $Y(K\alpha)$ with a corresponding steep decrease of $Y(K\beta)$ which reaches zero for $Z^* > 18$ where the $3p$ shell is empty.

The transition array average energies $E(K\alpha \text{ or } K\beta; Z^*)$ have been in turn evaluated from the fine-structure transition energies $E(i, j; Z^*)$, of Ref. [32] and from the fine-structure fluorescence yields calculated by Eq. (4) using the formula given below:

$$E(K\alpha \text{ or } K\beta;\ Z^*) = \frac{\sum_{i,\,j\in(K\alpha \text{ or } K\beta)} E(i,\ j;\ Z^*)\, Y(i,\ j;\ Z^*)}{\sum_{i,\ j\in(K\alpha \text{ or } K\beta)} Y(i,\ j;\ Z^*)}. \quad (5)$$

Our $K\alpha$ emission (average) energies as calculated using Eq. (5) have been compared with those of the FLYCHK code [33] in Fig. 3, where, for $Z^* < 20$, $K\alpha_1$ and $K\alpha_2$ transition arrays have been distinguished to facilitate the comparison. For $Z^* > 20$, the average energy value of the $K\alpha$ lines is provided for simplicity. One can see a good agreement although a slight redshift is predicted by the data of Ref. [32] as the charge state goes from 0 to 12, as is experimentally confirmed for other elements (iron, nickel, and titanium) by Aglistkii *et al.* [34].

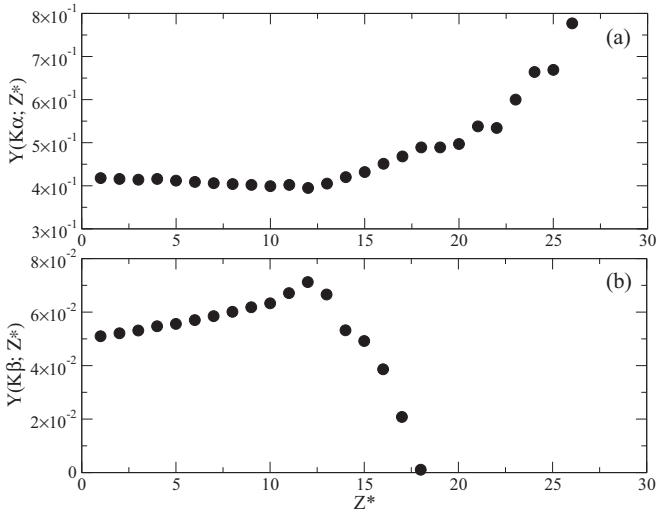

FIG. 2. Average fluorescence yield (in %) of (a) $K\alpha$ and (b) $K\beta$ transition arrays as functions of the charge state Z^*.

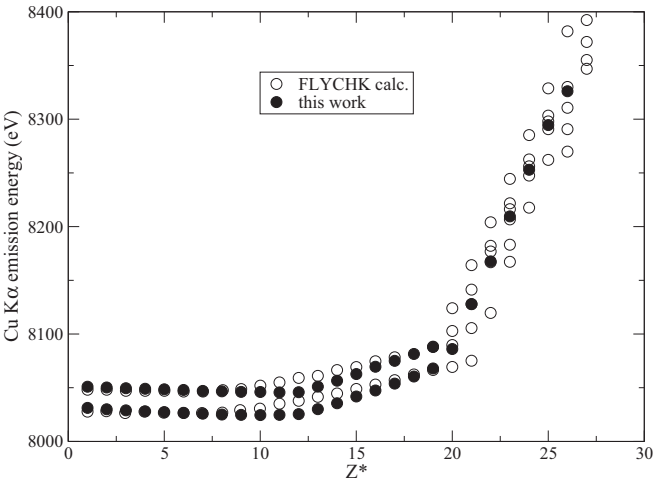

FIG. 3. Comparison of $K\alpha$ emission energies as calculated from Eq. (5) with those of FLYCHK [33].

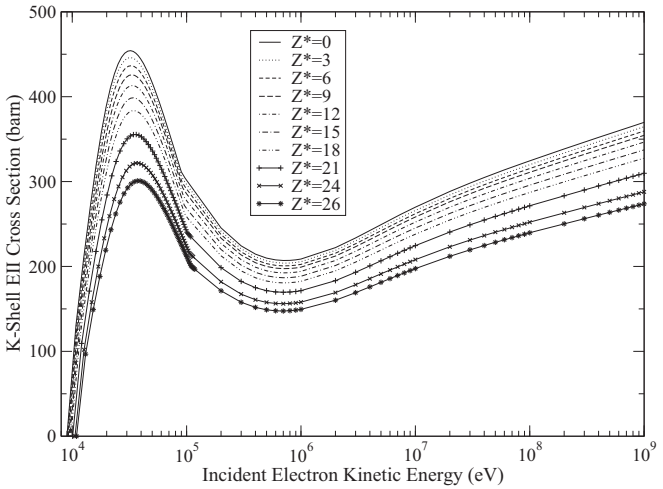

FIG. 4. Total K-shell electron impact cross sections of the ground states of ions of charge states Z^* plotted as functions of the incident electron kinetic energy.

Concerning the ground level total KEII cross sections $\sigma_K(E;\, Z^*)$, they have been estimated for each ion charge state Z^* as the sum over all partial KEII cross sections $\sigma_K(E;\, 1,\, j,\, Z^*)$, of fine-structure transitions from the parent ion (here, with charge Z^*) ground level $i = 1$ to all the possible final daughter ion (here, with charge $Z^* + 1$) K-vacancy levels j as given in Ref. [31]:

$$\sigma_K(E;\, Z^*) = \sum_j \sigma_K(E;\, 1,\, j,\, Z^*). \tag{6}$$

In Fig. 4, we have plotted all the total KEII cross sections for each charge state as functions of incident electron kinetic energy. One can see that the threshold energies increase with Z^* from ∼8 to ∼10 keV and the cross sections decrease with Z^* [31].

In Fig. 5, the ratios with respect to $Z^* = 0$ of the KEII cross sections taken at the 30 keV peak energy and of the fluorescence yields are presented as functions of Z^*. The decreasing trend is quite smooth for the cross section (the overall decrease is ≈30%), while it is relatively steeper for the fluorescence yields. In the case of $K\alpha$, it follows pretty well the cross section trend up to $Z^* = 12$ and then steeply increases up to a factor of ≈2. From this figure, it is clear that for the low- to moderate-charged ions ($Z^* < 18$) the $K\beta$ emission yield will be more sensitive to the mean charge state of the plasma, i.e., to the ionization balance and therefore to the plasma temperature. For plasma temperatures where the ions with $Z^* > 18$ dominate, the $K\alpha$ emission yield is expected to be a good diagnostic for plasma temperature. Ranges of Z^* where a specific subshell is last occupied are also displayed in the figure. This shows that the $K\alpha$ fluorescence yield starts to increase and the corresponding $K\beta$ fluorescence yield starts to decrease when the $3p$ subshell starts to be open.

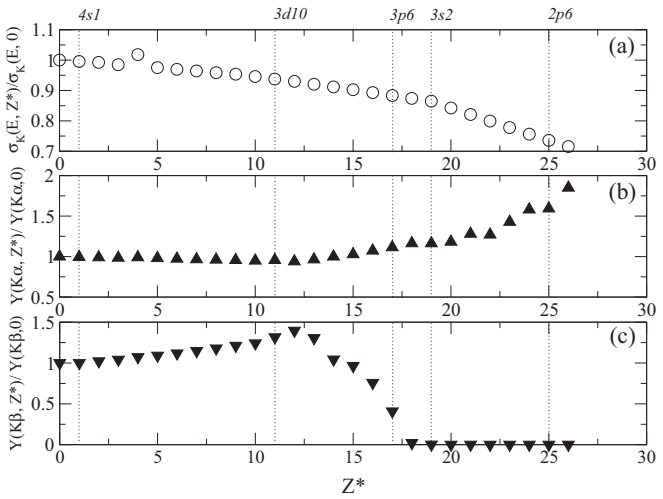

FIG. 5. Ratios with respect to (a) neutral species for the KEII cross section at the 30 keV peak energy, and (b) the $K\alpha$ and (c) $K\beta$ fluorescence yields as functions of charge states Z^*.

IV. INFLUENCE OF TARGET HEATING ON $K\alpha$ AND $K\beta$ OBSERVABLES

We performed Monte Carlo GEANT4 [35] simulations to predict the number of $K\alpha$ and $K\beta$ photons produced in a 10-μm-thick Cu target due to hot electrons produced in the laser-plasma interaction. Usually these electrons are characterized by a distribution function $f(E)$, which is often represented as a Maxwellian, or more simply an exponential slope. At high intensity a relativistic Maxwellian (Jüttner distribution) is used [36]. In the following we have used for simplicity exponential functions:

$$f(E) = f_0 \exp\left(-\frac{E}{T_{\rm hot}}\right), \tag{7}$$

where $T_{\rm hot}$ is the average energy of the distribution (this is often referred to as the "temperature" in the literature; however, let us notice that for a Maxwellian distribution the average energy is $3T_{\rm hot}/2$ while for an exponential distribution it is $T_{\rm hot}$. We have studied two cases $T_{\rm hot} = 50$ keV and $T_{\rm hot} = 500$ keV as representative cases of hot electrons which may be produced in the interaction with matter of nonrelativistic lasers (such as those which can be used in shock ignition experiments [37]) and of hot electrons produced in relativistic interaction with high-intensity lasers, such as those which should be studied in fast-ignition experiments [38].

Using for instance the LIVERMORE [39] or PENELOPE [40,41] physics library, GEANT4 allows simulation of the atomic deexcitation within materials. To investigate the influence of target heating on the $K\alpha$ and $K\beta$ production, we performed individual simulations for each Z^* by using $\sigma_K(E;\, Z^*)$ and $Y(K\alpha$ or $K\beta,\, Z^*)$ presented in the previous section. As illustrated in Fig. 6, we calculated the $K\alpha$ and $K\beta$ intensities at different Z^* and normalized them per joule of incident electrons.

Simulation results show that, first, when we change the initial electron temperature $T_{\rm hot}$, the absolute $K\alpha$ and $K\beta$ intensities change. This is due to the fact that distributions with different temperatures have a different number of electrons with energies which are more effective in producing inner shell ionization (and then emission of characteristic lines). Second, when we change Z^* for a given $T_{\rm hot}$, the $K\alpha$ intensity is found

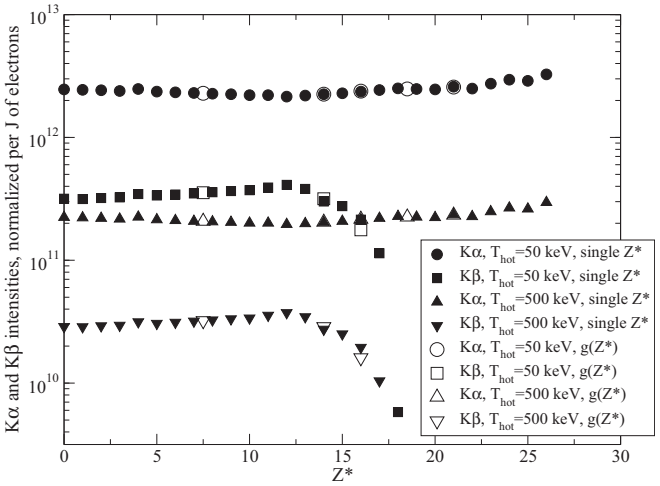

FIG. 6. Monte Carlo simulations of $K\alpha$ and $K\beta$ intensities generated within a $10-\mu$m-thick Cu target assuming an input exponential electron distribution with $T_{\rm hot} = 50$ keV and 500 keV. $K\alpha$ and $K\beta$ intensities are normalized per J of incident electrons. Full symbols correspond to calculations made for individual Z^* while empty symbols correspond to Z^*-averaged calculations over the realistic ion distribution of Fig. 9.

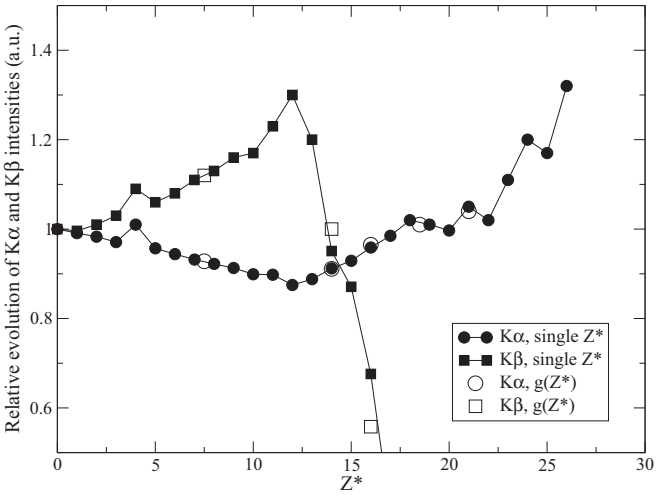

FIG. 7. Evolution of $K\alpha$ and $K\beta$ intensities as functions of Z^* with respect to cold matter (i.e., with $Z^* = 0$). Full symbols correspond to calculations made for individual Z^* while empty symbols correspond to Z^*-averaged calculations over the realistic ion distribution of Fig. 9.

to decrease slightly up to $Z^* = 12$ and then rises by up to a factor of 2 at higher Z^*, while the $K\beta$ intensity increases with Z^* below $Z^* = 12$ and then collapses above.

We also observe that the relative behavior of $K\alpha$ and $K\beta$ intensities is quasi-independent of $f(E)$. within a few percent. This can be rather simply understood since for the following reasons:

(1) When Z^* is changed, $\sigma_K(E;\, Z^*)$ has a shift that is almost exactly the same all over the energy range (of course this is not true at the threshold energy but the shift of the binding energy when Z^* is increasing is found to be lower than 2 keV over the whole Z^* range).

(2) $Y(K\alpha,\, Z^*)$ and $Y(K\beta,\, Z^*)$ are independent of the incident electron kinetic energy.

The relative behavior of $K\alpha$ and $K\beta$ intensities, illustrated in Fig. 7, can hence be assumed to be independent of $T_{\rm hot}$. The $K\alpha$ production decreases by 10% for $Z^* < 12$, and then slightly rises above. For instance, at $Z^* = 25$, the $K\alpha$ intensity is higher by 20% with respect to what happens in a cold copper target, i.e., at $Z^* = 0$. On the other hand, the $K\beta$ intensity is found to change more drastically: it increases by 30% from $Z^* = 0$ to $Z^* = 12$. Therefore, the $K\beta$ emission is more sensitive than $K\alpha$ to the changes in Z^* in the latter range. However, for $Z^* > 15$, the $K\beta$ emission practically disappears so it can no longer be used as a diagnostic. Note that, in terms of plasma temperature, $Z^* = 15$ corresponds to nearly $T = 150$ eV (as calculated with FLYCHK [33]).

In Fig. 8, we give the calculated $K\alpha/K\beta$ ratio as a function of Z^*. This relative value is also independent of $f(E)$ but is sensitive to Z^*. A slight decrease is observed for $Z^* < 13$. That is why the $K\alpha/K\beta$ ratio could be a relevant observable for studying warm dense matter with temperatures below $T = 100$ eV. For $12 < Z^* < 18$, the ratio can also be used to diagnose the plasma up to $T = 400$ eV. However, above this temperature, the $K\beta$ production becomes negligible and the $K\alpha/K\beta$ ratio tends to $+\infty$.

In the following, we will discuss the effect of target ionization under "realistic" conditions on the $K\alpha$ and $K\beta$ emission. Up to now, in this paper, we have studied the case in which the atoms in the targets all have the same ionization state. But, in reality for a given temperature, and hence a given average ionization Z^*, there will be an ionization equilibrium in the material with several ionization states simultaneously present. Such equilibrium will be described by a Saha-like equation with corrections for high density and electron degeneration. The ionization state Z^* as a function of the temperature of the target background material is shown in

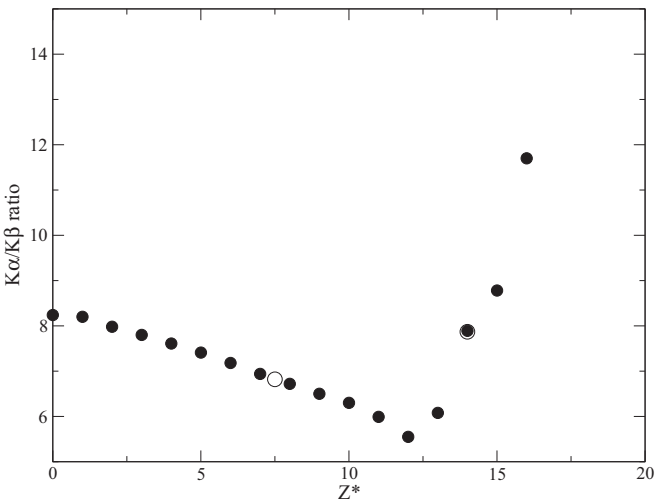

FIG. 8. Evolution of $K\alpha/K\beta$ ratio as a function of Z^*. Full circles correspond to calculations made for individual Z^* while empty circles correspond to Z^* averaged calculations over the realistic ion distribution of Fig. 9.

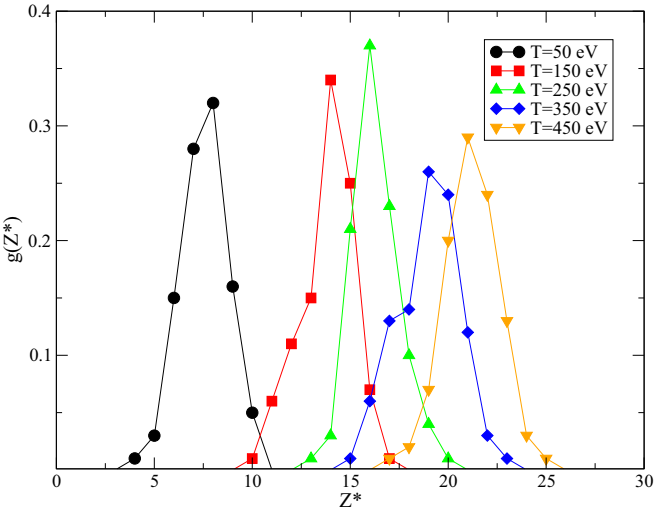

FIG. 9. (Color online) Ionic charge Z^* distribution as calculated by FLYCHK [33] for different target temperatures T at $N_e = 10^{19}/\mathrm{cm}^3$.

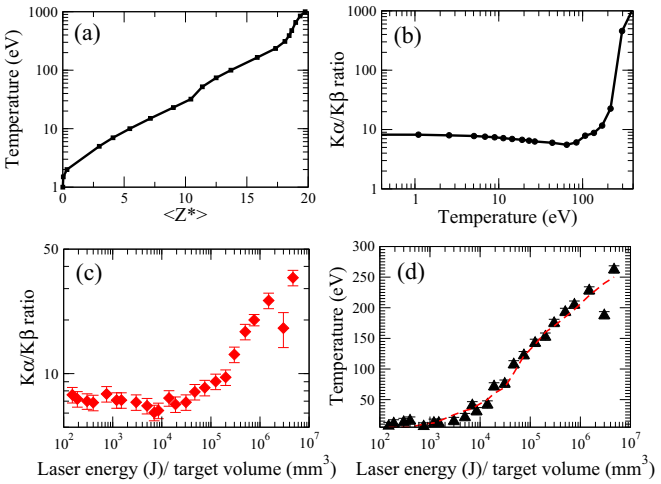

FIG. 10. (Color online) (a) Temperature T vs mean ionization state $\langle Z^* \rangle$, as calculated by FLYCHK; (b) $K\alpha/K\beta$ ratio as a function of Z^*, deduced from Figs. 8 and 10(a); (c) experimental data for the $K\alpha/K\beta$ ratio as a function of energy density (J/mm^3), as taken from [42]; (d) bulk temperature inferred using our calculations (full triangles) compared to results given in [42] (dashed line).

Fig. 9 calculated with FLYCHK [33] for $T = 50, 150, 250, 350,$ and 450 eV and $N_e = 10^{19}/\mathrm{cm}^3$, where N_e is the electron density. These are temperatures which can really be reached in experiments, especially the lowest ones, and for which at the same time we see a big change of Z^*.

When we deal with such realistic conditions and the simultaneous presence of several ionization states, the emission and shift of characteristic lines will need to be averaged over the ion distribution. We have done this using the $g(Z^*)$ distributions from Fig. 9. Corresponding results are shown using empty circles in Fig. 6, 7, and 8, where Z^* corresponds to the mean value of $g(Z^*)$. We notice that in general the shift of all quantities is negligible.

Let us notice again that the cases we have studied here are simple "school cases" in which the Cu layer is uniformly heated at a given temperature T. In the previous section we considered that the ionization state was also uniform inside the layer. Now we have used a statistical distribution $g(Z^*)$ of ionization states at the temperature T. But in no case have we tried to really simulate the real state of a target following laser irradiation and passage of hot electrons. In the "real" case we will have a distribution of temperatures inside the targets, bringing a much more complicated situation. But the general trends remain the same and, indeed, they are better evidenced by studying such simpler school cases.

V. APPLICATION TO EXISTING DATA

In this section, we use data from [42] in order to support our theoretical calculation and illustrate how it could be useful for temperature diagnostics in laser-plasma experiments. In [42], Nilson *et al.* studied the interaction of small-mass copper foil targets with a high-intensity 10^{19}W/cm^2 laser pulse. K-shell x-ray spectroscopy was used to infer the bulk temperature. By changing the geometry of the target (both thickness and surface), the fast-electron refluxing and hence the energy density within the target were modified. Since the geometry of the target was not fixed, the $K\beta$ and $K\alpha$ absolute intensities cannot be used to diagnose the temperature. That is why the temperature was inferred by measuring the strong modification of the cold $K\beta$ photon fluorescent probability suppression with increasing energy density, through strong modification of the cold $K\beta/K\alpha$ ratio. The relation between bulk temperature and the cold $K\beta/K\alpha$ was based on hybrid particle-in-cell simulations coupled to a K-photon production model, not detailed by the authors. By making use of their data, we applied our theoretical calculations to deduce the bulk temperature. In Fig. 8, we already gave the evolution of the $K\alpha/K\beta$ ratio as a function of Z^*. In addition, we performed FLYCHK calculations to link the mean ionization state $\langle Z^* \rangle$ with a plasma temperature T; see Fig. 10(a). This enables us to infer a direct relation between the $K\alpha/K\beta$ ratio and the temperature; see Fig. 10(b). In Fig. 10(c), we report the experimental $K\alpha/K\beta$ ratio as a function of the energy density within the target (J/mm^3), as measured in [42]. It can be seen that the $K\alpha/K\beta$ ratio is found to decrease first when the energy density is increased up to 10^4 J/mm^3 and then it increases strongly above this limit. The data follow the same behavior as our theoretical predictions as a function of Z^* (Fig. 8) and T [Fig. 10(b)]. In Fig. 10(d), we deduced the bulk temperature from the $K\alpha/K\beta$ ratio (full triangles) and compared our results to those obtained in [42] (dashed line). An excellent agreement is found. However, we believe that our temperature determination is more accurate than that in [42]. Indeed, at low temperature, i.e., where $T < 50$ eV, Nilson *et al.* did not take into account the decrease of the $K\alpha/K\beta$ ratio. Our theoretical calculations show that this effect should not be neglected. At higher temperature, when the $K\beta$ transitions become improbable, our temperature determination through the $K\alpha/K\beta$ increase is very similar to that in [42]. As a conclusion, this comparison demonstrates that our calculations could be used as a generic theoretical background for temperature diagnostics in laser-plasma interactions.

VI. CONCLUSIONS

In this paper, starting from first principles, we have studied the problem of the shift of characteristic lines ($K\alpha$ and $K\beta$), the ionization cross section, and fluorescence yield vs ionization induced by target heating. We have compared our results with those provided by the numerical code FLYCHK and we have found a good agreement, although the redshift at low charge states ($Z^* < 12$) is not predicted by FLYCHK.

The shift in emission is an already known issue. On one side, it can be the basis of so-called "$K\alpha$ spectroscopy", i.e., the analysis of the $K\alpha$ wavelength and line shape to recover the temperature of the background material. On the other side, it is well known to bring to experimental problems in the case in which monochromatic x-ray imagers are used (the shift may be significant with respect to the instrument bandwidth and may "blind" the instrument). Concerning the ionization cross section, there is a small shift to higher electron energies in both the ionization threshold and the maximum of the function. However, this shift is small and balanced by the fact that the fluorescence yield change has an opposite trend. To study the effects on $K\alpha$ and $K\beta$ intensities, we implemented Z^*-dependent atomic data in the Monte-Carlo GEANT4 code. A change of the total number of emitted photons is clearly highlighted as a function of Z^*. This change is in general more drastic for $K\beta$ photons. This trend is true for both monoenergetic electrons and for the more realistic case in which we consider an electron energy distribution function, as is really produced in laser-plasma experiments.

A clear signature of the atomic shell structure is recognizable in the behavior of the fluorescence yields. For instance, the $K\alpha$ yield begins to increase more when the shell $3p$ begins to open. As for the $K\beta$ yield it increases when the $3d$ shell opens and sharply decreases when the $3p$ shell opens, due to the dramatic loss of electrons, which can cause the $K\beta$ transition following ionization. Indeed, the almost total disappearance of $K\beta$ for ionization states larger than $Z^* \approx 16$ allows for more sensitive diagnostics of the target background temperature. In particular the $K\alpha/K\beta$ ratio will allow measurement of Z^* and temperature without the need for an absolute calibration (measurement of absolute photon yields).

We also showed that the total $K\alpha$ and $K\beta$ photon emissions (and their ratio) are not really sensitive to the changes in the hot electron temperature $T_{\rm hot}$, nor to the details of the energy distribution of ionic states in the target, $g(Z^*)$. This means that the total number of emitted photons will not change if we consider the target uniformly ionized with only one ionization state, or we consider the real distribution of ionic states corresponding to the temperature of the material. Of course, instead the detailed line shape will be sensitive to $g(Z^*)$ because different ions will contribute to emitting $K\alpha$ (or $K\beta$) photons of different wavelengths, therefore producing changes in line shape and a line broadening.

In addition, we confronted our theoretical calculations with existing data provided by Nilson *et al.* [42]. We used the modification of the $K\alpha/K\beta$ ratio to infer the bulk temperature as a function of the energy density within a target. We demonstrated that our calculations can be used as a generic tool for temperature diagnostics in laser-plasma interactions.

Finally we notice that all the changes become more pronounced as we approach the limit of large temperature and ionization becomes larger (let us say $Z^* \approx 20$ and $T \geqslant 500$ eV). In this range $K\beta$ emission disappears and the $K\alpha$ yield has a more pronounced shift. Also the emitted $K\alpha$ spectrum becomes more complicated and is characterized by the presence of multiple "thermal" satellites (in the limit where Z^* is very large, lithiumlike, hydroge-like, and heliumlike ions are present and the emitted spectra become "thermal"). These effects will need to be considered carefully when new-generation lasers with short-pulse and larger energy (e.g. PETAL in France [43]) become available, allowing "isochoric heating" experiments to be performed at much higher temperaturesthan are possible now.

ACKNOWLEDGMENTS

Financial support from the Belgian FRS-FNRS is acknowledged. P.Q. and P.P. acknowledge support as, respectively, Research Director and Research Associate of this organization. The authors also acknowledge the support of the COST Action MP1208 "Developing the Physics and the Scientific Community for Inertial Fusion" as well as the EquipEx PETAL+, Contract No. ANR-10-EQPX-0048.

[1] A. Zigler, H. Zmora, and J. L. Schwob, The origin of K_α radiation in laser-produced aluminum plasma, Phys. Lett. A **63**, 275 (1977).

[2] J. D. Hares, J. D. Kilkenny, M. H. Key, and J. G. Lunney, Measurement of Fast-Electron Energy Spectra and Preheating in Laser-Irradiated Targets, Phys. Rev. Lett. **42**, 1216 (1979).

[3] D. Bond *et al.*, A measurement of the reduction of the range of fast electrons from laser irradiated targets due to density structure in low density gold substrates, Plasma Phys. **24**, 91 (1982).

[4] J. P. Freidberg, R. W. Mitchell, R. L. Morse, and L. I. Rudsinski, Resonant Absorption of Laser Light by Plasma Targets, Phys. Rev. Lett. **28**, 795 (1972).

[5] W. L. Kruer, *The Physics of Laser Plasma Interactions* (Addison-Wesley, Reading, MA, 1988).

[6] S. C. Wilks, W. L. Kruer, M. Tabak, and A. B. Langdon, Absorption of Ultra-Intense Laser Pulses, Phys. Rev. Lett. **69**, 1383 (1992).

[7] F. Brunel, Not-So-Resonant, Resonant Absorption, Phys. Rev. Lett. **59**, 52 (1987).

[8] A. Ya. Faenov, T. A. Pikuz, V. Avrutin, N. Izyumskaya, L. Shabelnikov, E. Shulakov, and G. A. Kyrala, Hard x-ray imaging using free-standing spherically bent crystals, Rev. Sci. Instrum. **74**, 2224 (2003).

[9] S. A. Pikuz, T. A. Shelkovenko, V. M. Romanova, D. A. Hammer, A. Ya. Faenov, V. A. Dyakin, and T. A. Pikuz, High-luminosity monochromatic x-ray backlighting using an

incoherent plasma source to study extremely dense plasmas, Rev. Sci. Instrum. **68**, 740 (1997).

[10] T. A. Pikuz *et al.*, Bragg x-ray optics for imaging spectroscopy of plasma microsources, J. X-Ray Sci. Technol. **5**, 323 (1995).

[11] E. Martinolli *et al.*, Fast-electron transport and heating of solid targets in high-intensity laser interactions measured by K_α fluorescence, Phys. Rev. E **73**, 046402 (2006).

[12] K. U. Akli, M. H. Key, H. K. Chung, S. B. Hansen, R. R. Freeman, M. H. Chen, G. Gregori, S. Hatchett, D. Hey, N. Izumi, J. A. King, J. Kuba, P. Norreys, A. J. Mackinnon, C. D. Murphy, R. Snavely, R. Stepehens, C. Stoeckel, W. Theobald, and B. Zhang, Temperature sensitivity of Cu K_α imaging efficiency using a spherical Bragg reflecting crystal, Phys. Plasmas **14**, 023102 (2007).

[13] W. Theobald *et al.*, Hot surface ionic line emission and cold *K*-inner shell emission from petawatt-laser-irradiated Cu foil targets, Phys. Plasmas **13**, 043102 (2006).

[14] S. B. Hansen *et al.*, Temperature determination using K_α spectra from M-shell Ti ions, Phys. Rev. E **72**, 036408 (2005).

[15] F. Amiranoff, K. Eidmann, R. Sigel, R. Fedosejevs, A. Maaswinkel, Yung-lu Teng, J. D. Kilkenny, J. D. Hares, D. K. Bradley, B. J. MacGowan, and T. J. Goldsack, The evolution of two-dimensional effects in fast-electron transport from high-intensity laser-plasma interactions, J. Phys. D: Appl. Phys. **15**, 2463 (1982).

[16] K. Terai, H. Daido, M. Fujita, F. Miki, S. Nakai, and C. Yamanaka, Lateral transport of hot electrons on a spherical target by 10.6-μm CO_2 laser irradiation, Appl. Phys. Lett. **46**, 355 (1985).

[17] L. Volpe, D. Batani, G. Birindelli, A. Morace, P. Carpeggiani, M. H. Xu, F. Liu, Y. Zhang, Z. Zhang, X. X. Lin, F. Liu, S. J. Wang, P. F. Zhu, L. M. Meng, Z. H. Wang, Y. T. Li, Z. M. Sheng, Z. Y. Wei, J. Zhang, J. J. Santos, and C. Spindloe, Propagation of a short-pulse laser-driven electron beam in matter, Phys. Plasmas **20**, 033105 (2013).

[18] T. Feurer, W. Theobald, R. Sauerbrey, I. Uschmann, D. Altenbernd, U. Teubner, P. Gibbon, E. Förster, G. Malka, and J. L. Miquel, Onset of diffuse reflectivity and fast electron flux inhibition in 528-nm-laser–solid interactions at ultrahigh intensity, Phys. Rev. E **56**, 4608 (1997).

[19] R. H. H. Scott *et al.*, A study of fast electron energy transport in relativistically intense laser-plasma interactions with large density scalelengths, Phys. Plasmas **19**, 053104 (2012).

[20] T. Yabuuchi *et al.*, Transport study of intense-laser-produced fast electrons in solid targets with a preplasma created by a long pulse laser, Phys. Plasmas **17**, 060704 (2010).

[21] J. S. Green *et al.* Effect of Laser Intensity on Fast-Electron-Beam Divergence Inssolid-Density Plasmas, Phys. Rev. Lett. **100**, 015003 (2008).

[22] P. Neumayer *et al.*, The role of hot electron refluxing in laser-generated K_α sources, Phys. Plasmas **17**, 103103 (2010).

[23] P. A. Norreys *et al.*, Integrated implosion/heating studies for advanced fast ignition, Phys. Plasmas **11**, 2746 (2004).

[24] A. Morace, L. Fedeli, D. Batani, S. Baton, F. N. Beg, S. Hulin, L. C. Jarrott, A. Margarit, M. Nakai, M. Nakatsutsumi, P. Nicolai, N. Piovella, M. S. Wei, X. Vaisseau, L. Volpe, and J. J. Santos, Development of x-ray radiography for high energy density physics, Phys. Plasmas **21**, 102712 (2014).

[25] T. Yabuuchi, H. Sawada, T. Bartal, D. Batani, L. A. Gizzi, M. H. Key, A. J. Mackinnon, H. S. McLean, P. A. Norreys, P. K. Patel, R. B. Stephens, C. Spindloe, W. Theobald, M. S. Wei, and F. N. Beg, Proton radiography of intense-laser-irradiated wire-attached cone targets, IEEE Trans. Plasma Sci. **39**, 2822 (2011).

[26] F. Perez, A. Debayle, J. Honrubia, M. Koenig, D. Batani, S. D. Baton, F. N. Beg, C. Benedetti, E. Brambrink, S. Chawla, F. Dorchies, C. Fourment, M. Galimberti, L. A. Gizzi, L. Gremillet, R. Heathcote, D. P. Higginson, S. Hulin, R. Jafer, P. Koester, L. Labate, K. L. Lancaster, A. J. MacKinnon, A. G. MacPhee, W. Nazarov, P. Nicolai, J. Pasley, R. Ramis, M. Richetta, J. J. Santos, A. Sgattoni, C. Spindloe, B. Vauzour, and L. Volpe, Magnetically-Guided Fast Electrons in Cylindrically-Compressed Matter, Phys. Rev. Lett. **107**, 065004 (2011).

[27] R. B. Stephens *et al.*, K_α Fluorescence measurement of relativistic electron transport in the context of fast ignition, Phys. Rev. E **69**, 066414 (2004).

[28] H. Sawada, W. Theobald, C. Stoeckl, G. Fiksel *et al.*, Monochromatic imaging of 8.0-keV Cu K_α emission induced by energetic electrons generated at OMEGA EP, IEEE Trans. Plasma Sci. **39**, 2816 (2011).

[29] D. Batani, L. Antonelli, S. Atzeni, J. Badziak, F. Baffigi, T. Chodukowski, F. Consoli, G. Cristoforetti, R. de Angelis, R. Dudzak, G. Folpini, L. Giuffrida, L. A. Gizzi, Z. Kalinowska, P. Koester, E. Krousky, M. Krus, L. Labate, T. Levato, Y. Maheut, G. Malka, D. Margarone, A. Marocchino, J. Nejdl, Ph. Nicolai, T. O'Dell, T. Pisarczyk, O. Renner, Y. J. Rhee, X. Ribeyre, M. Richetta, M. Rosinski, M. Sawicka, A. Schiavi, J. Skala, M. Smid, Ch. Spindloe, J. Ullschmied, A. Velyhan, and T.Vinci, Generation of high pressure shocks relevant to the shock-ignition intensity regime, Phys. Plasmas **21**, 032710 (2014).

[30] L. Antonelli, D. Batani, A. Patria, O. Ciricosta, C. Cecchetti, P. Koester, L. Labate, A. Giulietti, L. A. Gizzi, A. Moretti, M. Richetta, L. Giuffrida, L. Torrisi, M. Kozlova, J. Nejdl, M. Sawicka, D. Margarone, B. Rus, G. Schurtz, X. Ribeyre, M. Lafon, C. Spindloe, and T. O'Dell, Laser-plasma coupling in the shock- ignition intensity regime, Acta Tecnica **56**, T57 (2011).

[31] P. Palmeri, P. Quinet, and D. Batani, Copper fine-structure *K*-shell electron impact ionization cross sections for fast-electron diagnostic in laser-solid experiments, At. Data Nucl. Data Tables **102**, 1 (2015).

[32] P. Palmeri, P. Quinet, C. Mendoza, M. A. Bautista, J. Garcia, M. C. Witthoeft, and T. R. Kallman, Atomic decay data for modeling K lines of iron peak and light odd-Z elements, Astron. Astrophys. **543**, A44 (2012).

[33] H.-K. Chung, M. H. Chen, W. L. Morgan, Yu. Ralchenko, and R. W. Lee, FLYCHK: Generalized population kinetics and spectral model for rapid spectroscopic analysis for all elements, High Energy Density Phys. **1**, 3 (2005).

[34] E. V. Aglistkii *et al.*, The structure of $K\alpha$ and $K\beta$ lines radiated from highly ionised plasmas, J. Phys. B **15**, 2001 (1982).

[35] S. Agostinelli *et al.*, GEANT 4—a simulation toolkit, Nucl. Instrum. Methods Phys. Rev. A **506**, 250 (2003).

[36] T. P. Wright and G. R. Hadley, Relativistic distribution functions and applications to electron beams, Phys. Rev. A **12**, 686 (1975).

[37] S. Weber, C. Riconda, O. Klimo, A. Heron, and V. T. Tikhonchuk, Fast saturation of the two-plasmon-decay instability for shock-ignition conditions, Phys. Rev. E **85**, 016403 (2012).

[38] A. Debayle *et al.*, Characterization of laser-produced fast electron sources for fast ignition, Plasma Phys. Control. Fusion **52**, 124024 (2010).

[39] https://wci.llnl.gov/codes/tart/nuclearatomic.html

[40] J. Sempau *et al.*, An algorithm for Monte Carlo simulation of coupled electron-photon transport, Nucl. Instrum. Methods Phys. Res. B **132**, 377 (1997).

[41] J. Sempau *et al.*, Experimental benchmarks of the Monte Carlo code penelope, Nucl. Instrum. Methods Phys. Res. B **207**, 107 (2003).

[42] P. M. Nilson, W. Theobald, J. F. Myatt, C. Stoeckl, M. Storm, J. D. Zuegel, R. Betti, D. D. Meyerhofer, and T. C. Sangster, Bulk heating of solid-density plasmas during high-intensity-laser plasma interactions, Phys. Rev. E **79**, 016406 (2009).

[43] D. Batani, M. Koenig, J. L. Miquel, J. E. Ducret, E. d'Humieres, S. Hulin, J. Caron, J. L. Feugeas, Ph. Nicolai, V. Tikhonchuk, L. Serani, N. Blanchot, D. Raffestin, I. Thfoin, B. Rosse, C. Reverdin, A. Duval, F. Laniesse, A. Chancé, D. Dubreuil, B. Gastineau, J. C. Guillard, F. Harrault, D. Lebœuf, J.-M. Le Ster, C. Pès, J.-C. Toussaint, X. Leboeuf, L. Lecherbourg, and C. Szabo, Development of the PETawatt Aquitaine Laser system and new perspectives in physics, Phys. Scr. **T161**, 014016 (2014).